A unified mechanistic model for size-dependent deformation in nanocrystalline and nanotwinned metals

Pei Gu [a], Ming Dao [b,*], Robert J. Asaro [c], Subra Suresh [b]

[a] MSC Software Corporation, 6050 Scripps St., San Diego, CA 92122, USA
[b] Department of Materials Science and Engineering, Massachusetts Institute of Technology, Cambridge, MA 02139, USA
[c] Department of Structural Engineering, University of California, San Diego, La Jolla, CA 92093, USA

Abstract

We present a unified mechanistic model to rationalize size-dependent flow stress, activation volume and strain-rate sensitivity for metals with either nanocrystalline grains or nanoscale twins. The non-uniform partial dislocation model for flow stress [Asaro and Suresh, Acta Mater, Vol. 53, pp. 3369–3382, 2005; Gu et al., Scripta Mater, Vol. 62, pp. 361–364, 2010] is generalized here to consider both grain-size dependence and twin-thickness dependence of nanotwinned metals. A non-homogeneous nucleation model is proposed to predict the dependence of activation volume on both grain-size and twin-thickness. With the activation volume predicted from the non-homogeneous nucleation model and the flow stress obtained via the non-uniform partial dislocation model, strain-rate sensitivity as a function of characteristic structural length scale is also evaluated. This provides a unified approach from envisioning partial dislocation emission for the three size-dependent parameters characterizing the plastic deformation mechanism, flow stress, activation volume and strain-rate sensitivity, so that each one of these parameters is predicted when the geometry of the grains or nanotwins is known. The model predictions are shown to be consistent with a variety of available experimental data.
© 2011 Acta Materialia Inc. Published by Elsevier Ltd. All rights reserved.

Keywords: Nanostructured metals; Twinning; Flow stress; Strain rate sensitivity; Partial dislocation

1. Introduction

Plastic deformation of polycrystalline metals with grain size at the microscale is mainly controlled by intragranular lattice dislocations. When the grain size is refined into the nanoscale, typically below 100 nm, the abundance of grain boundaries provides barriers for intergranular dislocation motion, and the smaller grain size limits the scope of intragranular dislocation motion [1]. Such a change in deformation mechanism results in much higher strength, much lower activation volume and much higher strain-rate sensitivity for nanocrystalline materials compared with the microcrystalline materials [2–5]. Nanoscale twin lamellae embedded in ultrafine grains (typically a few hundred nanometers in size) can be introduced by means of pulsed electrodeposition [6]. These nanoscale twin lamellae provide coherent twin boundaries, i.e. the (1 1 1) planes of face-centered cubic (fcc) structures are crystallographic mirror planes. It has been shown that these twin structures with twin thickness at the nanoscale provide considerably higher ductility than nanocrystalline materials with a grain size similar to the twin thickness, in addition to a similar high strength [6–12].

The understanding of plastic deformation characteristics in nanocrystalline and nanotwinned materials, i.e. flow stress, activation volume and strain-rate sensitivity, is one of the major objectives in the ongoing investigation of nanoenhanced materials. In Refs. [2,3], an analytical model was developed for grain-size-dependent flow stress by envisioning the process of emitting partial dislocations from the grain boundary, which was observed in experiments and molecular dynamics (MD) simulations [6,13]. The model was later extended to consider a non-uniform partial

* Corresponding author. Tel.: +1 617 253 2100.
  E-mail addresses: pei.gu@mscsoftware.com (P. Gu), mingdao@mit.edu (M. Dao).

dislocation extension, and it was shown that the non-uniform partial dislocation model is more consistent with experimental data for the flow stresses of Cu and Pd [5]. The activation volume characterizing plastic deformation kinetics and strain-rate sensitivity characterizing the rate-controlling process are discussed in Refs. [3,4, 6–8,10,11,14–16] for nanocrystalline and nanotwinned metals. By evaluating the change of free energy around a crack-like stress concentrator near the nanoscale grain, a size-independent activation volume πb^3 (where b is the magnitude of the Burgers vector), consistent with the order of experimental data, was predicted in Ref. [3]. In this paper, we generalize the results from Refs. [3,5] to develop a non-homogeneous nucleation model to predict the size-dependent activation volume and strain-rate sensitivity, and to extend the non-uniform partial dislocation model for flow stress in nanocrystalline metals to nanotwinned metals. The model developed here for activation volume and strain-rate sensitivity, together with the models developed previously and here for flow stress [2,3,5], provide a unified approach for envisioning partial dislocation emission for these nanoscale quantities (flow stress, activation volume and strain-rate sensitivity), i.e. they can be predicted when grain size and twin thickness are known. These mechanistic models are formulated in terms of both grain size and twin thickness, and they are fully consistent with available experimental data.

In a thermally activated process contributing to plastic deformation, the activation volume is defined using the change of tensile strain rate $\dot\varepsilon$ with respect to tensile flow stress σ, the absolute temperature T and the Boltzmann constant k as [3]

$$V = \sqrt{3}kT\frac{\partial \ln \dot\varepsilon}{\partial \sigma}. \tag{1}$$

The strain-rate sensitivity, m, is related to the activation volume, V, by the expression:

$$m = \frac{\sqrt{3}kT}{V\sigma}. \tag{2}$$

Combining Eqs. (1) and (2), it is seen that the strain-rate sensitivity is essentially $m = \partial \ln \sigma / \partial \ln \dot\varepsilon$, which is consistent with the power law relationship of stress as a function of strain rate. As noted in the discussion below, V measures a physical volume in the thermally activated process that triggers considerable plastic flow. The inverse proportion of strain-rate sensitivity to activation volume is consistent with experimental data (e.g. [10]). Experimental measurements of plastic deformation at different strain rates, or different tests, e.g. stress-relaxation tests [11], are needed, in addition to uniaxial tensile tests, to determine the three quantities of interest: the flow stress, the activation volume and the strain-rate sensitivity. With the flow stress obtained from the partial dislocation model or the classical Hall–Petch relation [17,18] and the activation volume obtained from the non-homogeneous nucleation model, the strain-rate sensitivity is determined from Eq. (2). This provides

a means to theoretically evaluate the three parameters that characterize plastic deformation at the nanoscale. However, the free-energy approach in Ref. [3] results in a size-independent activation volume due to its over-restrictive requirement that both the free energy and the associated effective force reach maximum (Eqs. (30a,b) in Ref. [3]). In this paper, we formulate the free-energy approach that will lead to the evaluation of the size-dependent activation volume.

The outline of this paper is as follows. In Section 2, the non-uniform partial dislocation model for flow stress in nanocrystalline metals is extended to nanotwinned metals by considering representative partial dislocation extensions in the twin system. The predicted flow stress is compared with various experimental measurements reported for nanotwinned Cu. In Section 3, a concise review of mechanistic models for activation volume is given, and the non-homogeneous nucleation model to predict activation volume is developed. Using nanocrystalline Cu and nanotwinned Cu as illustrative examples, we show that the model prediction is consistent with all available experimental data for both activation volume and strain-rate sensitivity. This is followed by a concluding discussion and remarks that link the present general analysis to a variety of size-dependent deformation characteristics of nanocrystalline and nanotwinned materials.

2. Size-dependent flow stress in nanocrystalline and nanotwinned metals

In the non-uniform partial dislocation model [5], shear flow stress τ is expressed in terms of the stacking fault energy Γ, the magnitude of Burgers vector b, the shear modulus G, the grain size d and a parameter to measure the non-uniform extension β as

$$\frac{\tau}{G} = \frac{\Gamma}{Gb} + \left(\frac{1}{3} - \frac{1}{12\pi\beta}\right)\frac{b}{d}. \tag{3}$$

The parameter β is defined as $\beta = 1/d^2 \int_0^d \delta(x)dx$, where the extension distance $\delta(x)$ is non-uniform along the original dislocation line (grain boundary), and is related to the grain size. Eq. (3) clearly shows the dependence of flow stress on grain size, whereas the expressions in Refs. [2,3] arrange flow stress in two terms which incorporate the contributions of side segments and stacking fault. By appropriately choosing β, the flow stress can be shown to vary linearly with $d^{-0.5}$, similar to the so-called Hall–Petch relation, $\tau = k_0 + k_1 d^{-0.5}$, where k_0 and k_1 are Hall–Petch constants. Recasting Eq. (3) so that it is equivalent to the Hall–Petch relation, the following condition is obtained [5]:

$$\beta = \frac{1}{4\pi} \frac{1}{1 - 3\frac{k_1}{G\sqrt{b}}\sqrt{\frac{d}{b}}}. \tag{4}$$

Equating the grain-size-independent term of the Eq. (3) to that of the Hall–Petch relation, we note that $\Gamma = Gbk_0$. The stacking fault energy calculated from this relationship falls
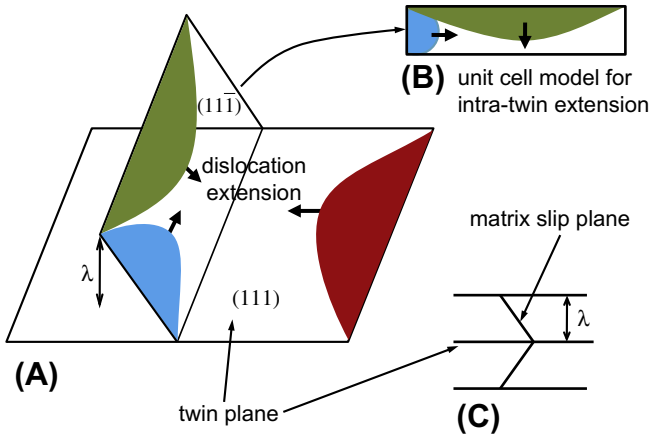
Fig. 1. Dislocation extensions on the twin boundary and matrix slip plane. According to the MD simulation [20], dislocation loops on the matrix slip planes are sources for strengthening (increasing strength with decreasing twin thickness); dislocation loops on the twin boundary are sources for softening (decreasing strength with decreasing twin thickness). Flow stress is evaluated from the unit cell model for intratwin slip.

into the expected range. For Cu, the stacking fault energy obtained from such approach is 34 mJ/m^2.

For the nanotwinned structures shown in Fig. 1, dislocation-mediated plastic deformation is active on the matrix slip plane for the strengthening mechanism to play a dominant role [6–8,10,19,20]. The partial dislocation extension along the transverse direction of the matrix slip plane (shown in green color) was considered in Refs. [7,8], whereas the partial dislocation extension parallel to the twin boundary (in blue color) was discussed in the molecular dynamics simulation in Ref. [20]. We generalize the non-uniform partial dislocation extension model for nonacrystalline materials [5] to include nanotwinned materials by considering representative intratwin extensions: the partial dislocation loops toward and parallel to the twin boundary (the green and blue color loops in Fig. 1).

Let the shear stresses required to extend the partial dislocation loops toward and parallel to the twin boundary be τ_1 and τ_2, respectively; both can be obtained by the procedures outlined in Ref. [5]. The shear flow stress for the twin structure is regarded as lying in between the above two flow stresses and is estimated as $\tau = (\tau_1 + \tau_2)/2$, which gives

$$\frac{\tau}{G} = \frac{\Gamma}{Gb} + \frac{1}{2}\left(\frac{1}{3} - \frac{1}{12\pi\beta_1}\right)\frac{b}{\lambda_1} + \frac{1}{2}\left(\frac{1}{3} - \frac{1}{12\pi\beta_2}\right)\frac{b}{d}. \quad (5)$$

In this expression, there are two extension parameters, $\beta_1 = 1/(\lambda_1 d)\int_0^d \delta_1(x)dx$ and $\beta_2 = 1/(\lambda_1 d)\int_0^{\lambda_1}\delta_2(x)dx$, with $\lambda_1 = \lambda/\sin\theta$ and $\theta = 70°$ being the angle between the matrix slip plane and the twin boundary. Both extension parameters are related to the geometrical lengths, grain size d and twin thickness λ, and so is the flow stress. In the numerics that follow, we use the approximation $\lambda_1 \approx \lambda$.

The shear flow stress model in Eq. (5) is developed by recognizing intratwin dislocation extension, whereas the shear flow stress model in Eq. (3) is derived by recognizing intragranular dislocation extension. Eq. (5) shows that

both twin thickness and grain size contribute to the shear flow stress of nanotwins. For large grain size, the third term on the right-hand side is ignored such that the twin thickness is similar to the grain size in Eq. (3) for nanocrystalline materials. If $\beta_1 = \beta_2$, $d = 400$ nm and $\lambda = 20$ nm, the magnitude of the third term is only 5% of the second. Note from prior work [9–11] that the effect of twin thickness for nanotwinned copper (with a fixed grain size of ~500 nm) was found to be equivalent to that of the grain size for nanocrystalline copper in relation to their respective size dependence of flow stress. Here the flow stress, activation volume and strain-rate sensitivity vs. twin thickness for nanotwins provide good correlation for size dependence of the same parameters when the grain size is used for nanograins as a characteristic size scale. In such cases, the effects of twin thickness on mechanical response are similar to those seen as a function of grain size. In Eq. (5), for the case without nanotwins, $\lambda = d$ and $\beta_1 = \beta_2$ such that it recovers Eq. (3) for the flow stress in nanocrystalline metals.

If the Hall–Petch-type relation for nanotwins can be written as $\tau = k_0 + k_1^*\lambda^{-0.5} + k_1 d^{-0.5}$, β_1 and β_2 can be recast from Eq. (5) to be equivalent to the Hall–Petch-type relation:

$$\beta_1 = \frac{1}{4\pi}\frac{1}{1 - 6\frac{k_1^*}{G\sqrt{b}}\sqrt{\frac{\lambda}{b}}}; \quad \beta_2 = \frac{1}{4\pi}\frac{1}{1 - 6\frac{k_1}{G\sqrt{b}}\sqrt{\frac{d}{b}}}. \quad (6)$$

At the intersection of the twin boundary and the matrix slip plane, various situations for absorption of the dislocations onto the twin boundary or transmission of the dislocations onto the adjacent matrix slip plane have been envisioned in the MD simulations and multiscale simulations [7,21–24]. A cross-slip model [8] gives a simple criterion: $\sqrt{3}\pi\tau^2\lambda/(Gb) \pm 0.65\tau = 0.024G$, where the plus sign is for absorption, the minus sign is for transmission, and G is the shear modulus.

Once the twin size becomes very small (on the order of ~10 nm or less), the flow stress of a nanotwinned metal instead decreases along with the twin thickness, just as the flow stress of a nanocrystalline material drops below a critical nanograin size of comparable magnitude; this phenomenon of softening with feature-size refinement is known as strength softening, or inverse Hall–Petch behavior [9,25]. In this situation, an active plastic deformation mechanism results from the dislocation nucleation and extension on the twin boundary (red colored loop in Fig. 1), instead of those dislocations on the matrix slip plane, and from the thermal activation equation the flow stress in the strength softening is expressed as [20]

$$\tau = \frac{Q}{SV} - \frac{kT}{SV}\ln\left(\frac{d}{\lambda}\frac{v_D}{\dot{\varepsilon}}\right). \quad (7)$$

In the above expression, Q is the activation energy, S is a scalar representing local stress and geometry, V is the activation volume, v_D is the Debye frequency and $\dot{\varepsilon}$ is the strain rate. The values chosen for these constants are

$Q = 1$ eV, $S = 0.25$, $V = 2.4\Omega_0$ (with Ω_0 being the atomic volume) and $v_D = 1.3 \times 10^{13}$ s^{-1}. For nanocrystalline metals, inverse Hall–Petch behavior is associated with grain rotation to a larger extent than with dislocation nucleation at the grain boundary [26].

The typical material properties for Cu are $G = 50$ GPa, $b = 0.255$ nm and $\Gamma/(Gb) = 0.00425$. Taking the non-uniform partial dislocation extension parameter β to be 0.18, the shear flow stress calculated from Eq. (3) is plotted in Fig. 2 against experimental data of nanocrystalline Cu, which are recompiled from those plotted in Fig. 3 of Ref. [5]. The Hall–Petch fit is also shown in Fig. 2, which gives the coefficient for the constant term $k_0 = 0.128$ GPa and the coefficient for the grain-size-dependent term $k_1 = 0.97$ GPa nm$^{0.5}$. The shear flow stress for nanotwinned Cu with $d = 500$ nm is plotted in Fig. 3 against the twin thickness and experimental data given in Ref. [9], using

Fig. 2. Shear flow stress of nanocrystalline Cu predicted from the non-uniform partial dislocation model and Hall–Petch relation. Data are recompiled from Ref. [5].

Fig. 3. Shear flow stress of nanotwinned Cu predicted from the non-uniform partial dislocation model is compared with that measured in experiments in Ref. [9].

expressions (5) and (7). For simplicity, we choose $\beta_1 = \beta_2 = 0.204$, which is obtained by fitting the data around $\lambda = 16$ nm. The intersection of the two curves (blue and red) in Fig. 3, which is indicated by an open diamond symbol, is where strength softening occurs. The critical twin size is around 14.25 nm, which is comparable to the critical grain size for the transition in nanocrystalline Gu. From the two figures, for both nanocrystalline and nanotwinned structures, the model prediction is consistent with experimental data. For strain-rate dependence, the extension parameters, β, β_1 and β_2, which also measure the side segments of the dislocations, can be related to the strain-rate sensitivity m. In Refs. [3,28], the side segments of the dislocations are envisioned to be affected by strain rate.

3. Size-dependence of activation volume and rate sensitivity

3.1. A size-dependent, non-homogeneous, partial dislocation model for activation volume

We begin with the examination of the free energy associated with the dislocation loop. The energy of a half-circular loop with radius r is [3,27]

$$U_1 = Gb^2 \frac{2-v}{8(1-v)} r \ln\left(\frac{r}{r_0}\right), \tag{8}$$

where b is the magnitude of the Burgers vector, r_0 is the core cut-off radius and v is Poisson's ratio. For homogeneous nucleation, i.e. for large grain size and no stress concentration, the energy associated with shear flow stress τ on the slip plane is

$$U_2 = \frac{1}{2}\tau\pi b(r^2 - r_0^2). \tag{9}$$

The free energy for the dislocation loop is $U = U_1 - U_2$. The energies created by a half-circular partial dislocation loop are estimated [3,27] by replacing b in the above expressions for the energy of perfect dislocation loop with $b_1 = b/\sqrt{3}$, the magnitude of Burgers vector for the partial dislocation. In considering non-homogeneous nucleation, a grain boundary facet crack was introduced [3] where the shear stress field on slip plane is $K_{II}/\sqrt{2\pi r}$ and $K_{II} = \tau\sqrt{\pi d/2}$. The size of a grain boundary facet crack approximates the grain size. The energy associated with the shear stress in the facet crack case is $U_2 = 1.4 K_{II} b_1 (r^{3/2} - r_0^{3/2})$. In addition, in the partial dislocation loop case, there is energy term associated with the creation of a stacking fault, which is expressed in terms of the stacking fault energy Γ as $U_3 = \frac{1}{2}\pi\Gamma(r^2 - r_0^2)$. The free energy for the partial dislocation loop is $U = U_1 - U_2 + U_3$. As r increases, the free energy U goes to a minimum and then a maximum. In Ref. [3], the critical loop radius r_c and the driving force K_{II} associated with the maximum of U were estimated by having both $\partial U/\partial r = 0$ and $\partial^2 U/\partial r^2 = 0$. This leads to the result that the activation volume is grain-size independent, i.e. $V = \pi b^3$. This estimate correctly predicts the order of activation volume,
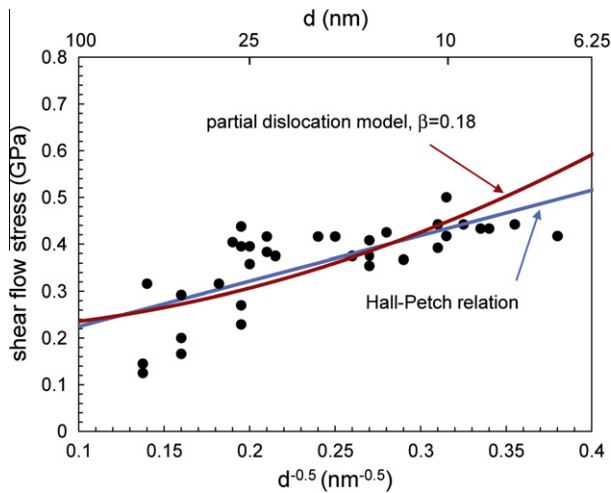
$$U = Br \ln\left(\frac{r}{r_0}\right) - \tau\pi\left(r^2 - r_0^2\right)$$
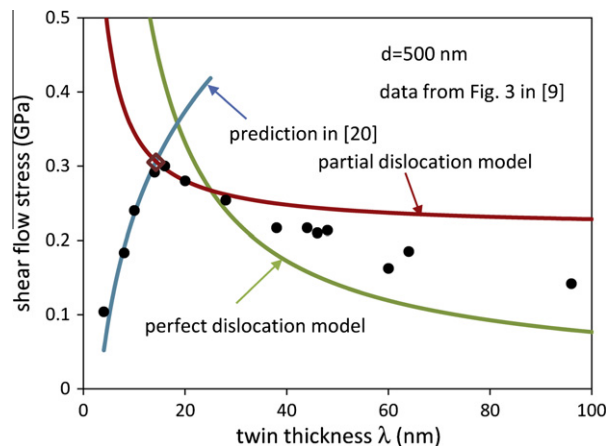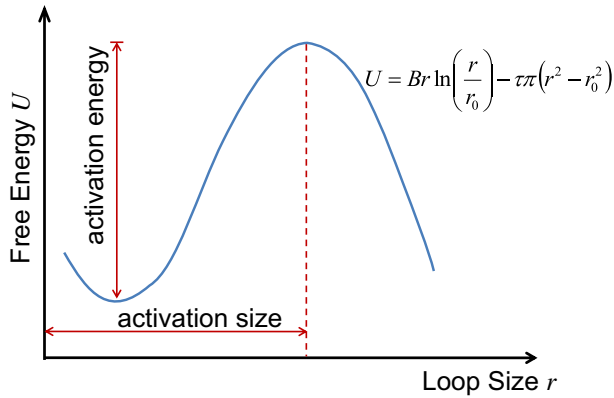
Fig. 4. Free energy path. The size of the loop, at which the first maximum of the free energy is attained in the region $r > 0$, is the size for activation. The first maximum is followed by the first minimum. When determining the activation size from $U'(r) = 0$, the second root from the left is the activation size r_c. The activation volume is $V = A(r_c)b = \pi r_c^2 b/2$.

as demonstrated by the data from nanoexperiments (e.g. [6,10]). As seen from Fig. 4, setting only the free energy to be maximum (i.e. $\partial U/\partial r = 0$) is sufficient to overcome the required activation energy.

In obtaining $V = \pi b^3$, the crack tip stress field, which is singular in the order of $1/\sqrt{r}$, was taken as the driving force. It is reasonable to probe the stress concentration because the misoriented structure of a grain boundary under deformation generates intense local stress concentration. The question then arises whether a grain boundary or its triple junction exhibits such a strong stress gradient. Recognizing this, Asaro and Suresh [3] discussed a homogeneous nucleation model for a perfect dislocation loop, where uniform shear stress on the slip plane was employed. With the free energy $U = U_1 - U_2$ and the energy from the uniform shear stress $U_2 = \frac{1}{2}\tau\pi b(r^2 - r_0^2)$, the requirement of maximum free energy, $\partial U/\partial r = 0$, gave a loop size for activation as

$$r_c = \frac{5}{16\pi}\left(\frac{\tau}{G}\right)^{-1} b[\ln(r_c/r_0) + 1]. \tag{10}$$

Note that, in obtaining the above expression, the over-restrictive requirement $\partial^2 U/\partial r^2 = 0$ is dropped. Substituting the simple estimation for flow stress $\tau/G = b/d$ into Eq. (10), it would be possible to obtain the size for activation in terms of grain size d from the algebraic equation. When we consider partial dislocation nucleation and neglect stacking fault energy for the time being, the above expression for the loop size at activation becomes

$$r_c = \alpha\left(\frac{\tau}{G}\right)^{-1} b\left(\ln\frac{\sqrt{3}r_c}{b} + 1\right). \tag{11}$$

In this expression, $\alpha = 5/(16\sqrt{3}\pi)$, and the core cut-off radius is taken to be $b/\sqrt{3}$; the shear flow stress τ is given by the models in the previous section, specifically Eqs. (3) and (5).

From Fig. 4, the activation energy is the first maximum free energy from the left minus the first minimum free energy from the left. Therefore, the loop size for activation is the second root of the algebraic equation, Eq. (11), in the region $r > 0$, and the activation volume is given by

$$V = \frac{1}{2}\pi r_c^2 b. \tag{12}$$

However, the value of α in Eq. (11), which is needed to determine r_c, is smaller in the case of non-homogeneous nucleation.

Consider that the partial dislocation loop is nucleated from a non-homogeneous source such as a grain boundary, where the shear stress in Eqs. (3) and (5) is enlarged by a concentration factor $\rho > 1$, i.e. the shear stress is approximately $\rho\tau$. Then, the same derivation leading to Eq. (11) gives $\alpha = 5/(16\sqrt{3}\pi\rho)$ for non-homogeneous nucleation. This tells that the larger the stress concentration, the smaller the non-homogeneous nucleation factor. Additionally, when the partial dislocation extends, there exists an interaction between the leading and trailing partial dislocations during the creation of the stacking fault. This interaction lowers the self-energy U_1 for the system, as seen in the Eq. (5) of Ref. [2] (the first term on the right-hand side), and thus can also result in a lower value for α.

We propose a non-homogeneous model for determining the activation volume where the loop size for activation is the second root of the Eq. (11) from the left of Fig. 4. In the non-homogeneous nucleation case, the shear stress in Eqs. (3) and (5) are employed for τ in Eq. (11). The non-homogeneous nucleation factor α is determined by evaluating the heterogeneous nature of the nanostructure at the nucleation site, or by fitting experimental data of activation volume. It is expected that the non-homogeneous nucleation factor is considerably less than $5/(16\sqrt{3}\pi)$. Note that, in deriving Eq. (11), we ignored the contribution to the energy from stacking fault, U_3. In other words, the non-homogeneous nucleation factor also accounts for the influence of the stacking fault, in addition to the influences of the stress concentration and dislocation loop interaction. More accurately, the stacking fault energy should be interpreted vis-à-vis unstable and stable stacking fault energies [3]. Due to the uncertainty of the data for unstable stacking fault energy, its contribution is represented in the non-homogeneous nucleation factor. In general, the non-homogeneous nucleation factor can be written as $\alpha = \alpha(\rho, b_1, b_2, \Gamma)$ (b_1 and b_2 are the magnitudes of the leading and trailing partial dislocations' Burgers vectors).

The above analysis qualitatively describes the role for the non-homogeneous nucleation factor α and also characterizes its numerical range.

In Ref. [8], the free energy for the perfect dislocation loop was used to model cross-slip (absorption vs. transmission) in nanotwinned grains, where a term for the energy of constricted segment along the intersection of two slip planes was included. The activation volume was evaluated

from the change of activation energy with respect to flow stress, $V = -\partial Q/\partial \tau$. The result estimated in this way is larger than that from atomistic reaction pathway calculations [7], which are more consistent with experimental measurement. Conrad [14] compared the expression for the change of strain rate with respect to stress (which is related to activation volume via thermal activation) with experimental data to estimate the activation volume. Although the correct order of magnitude estimate for activation volume was obtained, its grain-size dependence was not determined. Assuming a Hall–Petch relation for flow stress, Refs. [15,16] developed a Hall–Petch-type relation for $1/V$, where the Hall–Petch constants were expressed in terms of some internal variables, such as the activation volume for the grain boundary and the activation volume for the thermally activated flow of the entire grain. The Hall–Petch-type relation for the activation volume is not fully validated because of the scatter in experimental data around a Hall–Petch-type fitting line [10,11]. Nevertheless, the Hall–Petch relation for $1/V$ provides a basis for practitioners to fit their data using a straight line. As mentioned, Lu et al. [10,11] used the Hall–Petch-type relation to fit data for the activation volume.

3.2. Comparison of model prediction with experimental data

We chose Cu to validate the non-homogeneous model for nanocrystalline and nanotwinned structures because of the availability of experimental data for this fcc metal with both nanograins and nanotwins.

The material properties of nanocrystalline Cu are given in Section 2. Substituting the shear flow stress given by Eq. (3), where β is taken to be 0.18, into the expression (11), the size for activation, which is the second root of the resulting equation, is obtained using the Newton–Raphson scheme (which can be done by writing a simple program). The inverse of activation volume $1/V$ is plotted in Fig. 5 against
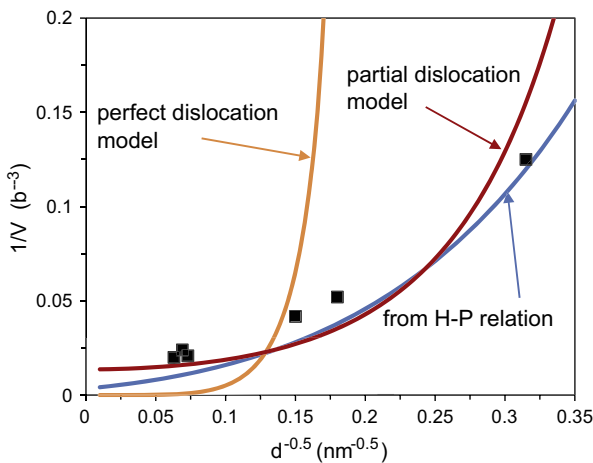
the inverse of the square root of grain size $d^{-0.5}$ and experimental data from Ref. [10]. The non-homogeneous nucleation factor α is chosen to be 0.0084 in fitting the experimental data, and this value falls into the range discussed in Section 3.1. We see that the activation volumes calculated from Eqs. (11) and (12) match the experimental data. The data on the left-hand side are for the grain size of around 270 nm, and the data on the right-hand side are for the grain size of around 10 nm. It appears that in some regions the activation volumes obtained by using the non-uniform partial dislocation model match the data better, whereas in others the activation volumes obtained by using the Hall–Petch relation for flow stress match the data better. However, the experimental measurements can be scattered along the vertical direction for the same grain size, as shown in Refs. [6,11]. The shear flow stress obtained from the perfect dislocation model, i.e. $\tau/G = b/d$, is also used in Eqs. (11) and (12) to calculate the activation volume. As shown in Fig. 5, the perfect dislocation model does not satisfactorily predict the activation volume at the nanoscale. The smaller the grain size, the larger the difference between the prediction of the perfect dislocation model and the experimental data. As seen in Figs. 2 and 5, only predictions from the non-uniform partial dislocation model and the Hall–Petch relation are consistent with the data. It was shown in Ref. [2] that the perfect dislocation model predicts unrealistically higher shear flow stress at the nanoscale.

For nanocrystalline materials, the shear flow stress (Eq. (3)) and the activation volume obtained from Eqs. (11) and (12) are substituted into Eq. (2) to calculate the strain-rate sensitivity, where the connection between the shear flow stress and the tensile flow stress is taken to be $\sigma = 2\tau$. Fig. 6 plots the strain-rate sensitivity exponent m against grain size on a logarithmic scale along with experimental data from Ref. [10]. The trends predicted by the model are again consistent with experimental data. The data on the left-hand side are for the grain size of around 10 nm,

Fig. 5. Activation volume vs. grain size for nanocrystalline Cu. The curves are predicted, and experimental data are from Ref. [10]. The nonhomogeneous nucleation factor is taken as 0.0084. The curve marked as "from H-P relation" is obtained by using the Hall–Petch fit for shear flow stress in Eqs. (11) and (12).
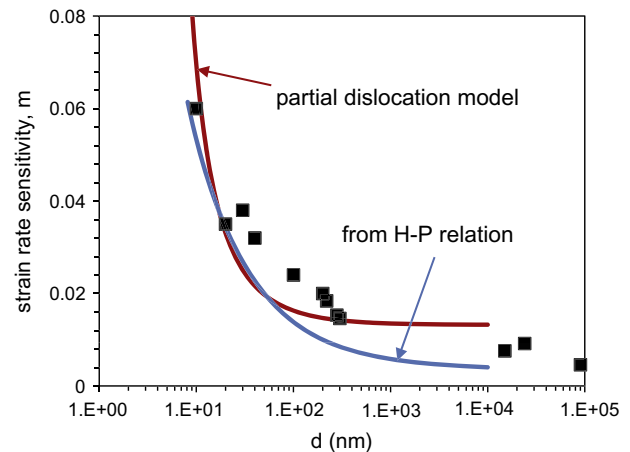
Fig. 6. Strain-rate sensitivity vs. grain size for nanocrystalline Cu. The curves are predicted, and experimental data are from Ref. [10]. The nonhomogeneous nucleation factor is taken as 0.0084.

and the data on the right-hand side are for the grain size of around 100,000 nm. In the region on the right-hand side well above the nanoscale, where the grain size is much larger than 100 nm, the prediction of the model developed for nanograins is not expected to match the experimental data. In the microcrystalline region, because large numbers of dislocations can be present in a grain, dislocation loop interactions may become significant such that the non-homogeneous nucleation factor α is no longer valid. This also raises questions about the accuracy in using the energy of a single loop to represent a system that has numerous dislocation loop interactions. In the microcrystalline region, dislocation cell structures [14] or dislocation pile-ups [27] would be expected to be present during plastic deformation. Note the similarity of the predicted curve in Fig. 6 with the curve in Fig. 1a of Ref. [10], which was obtained by simply fitting the strain-rate sensitivity data.

For nanotwinned Cu, the shear flow stress given by Eq. (5), where β_1 and β_2 are taken to be 0.205, is substituted into Eqs. (11) and (12) to calculate the activation volume and strain-rate sensitivity. Here, $\sigma = 3\tau$ is used to correlate the shear flow stress and tensile flow stress. The predicted activation volume and strain-rate sensitivity are plotted in Figs. 7 and 8 against experimental data taken from Table 2 in Ref. [11]. Again, the model predictions of both activation volume and strain-rate sensitivity for the nanotwinned Cu are consistent with experimental data. In the calculation, the non-homogeneous nucleation factor α is taken as 0.006 in fitting the experimental data, and this value is within the range discussed in Section 3.1. A decrease in the factor α from that for the nanocrystalline case (0.0084) can be expected since the stress concentration near the grain boundary in nanotwinned structures is higher than that in nanocrystalline structures due to the high aspect ratio of the edges of twins. However, this estimate is predicated upon continuum mechanics considerations. In addition, dislocations in nanotwinned Cu may
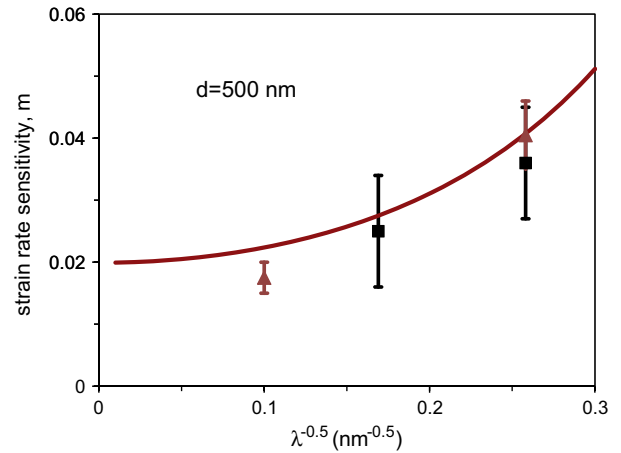
Fig. 8. Predicted and measured strain-rate sensitivity vs. twin thickness for nanotwinned Cu. The data are from Table 2 of Ref. [11]. The square symbols are from the nanoindentation test; the triangular symbols are from the jump test.

behave differently from those in nanocrystalline Cu [2–11,20], and such differences may have an influence on α. In other words, the fact that the α for nanotwinned Cu is different from that for nanocrystalline Cu may suggest different dislocation responses and different stress concentrations between the two nanostructures. Overall, the result in Figs. 5–8 shows that the non-homogeneous nucleation model can be used to estimate the trends in the size dependence of the activation volume and strain-rate sensitivity in both nanocrystalline and nanotwinned Cu. Future experimental data for other nanocrystalline and nanotwinned metals will elaborate the size dependence of these materials at the nanoscale, and should provide a further basis to assess the present model.

4. Concluding remarks

In summary, with the activation volume predicted from the non-homogeneous nucleation model and the flow stress obtained via the non-uniform partial dislocation model, strain-rate sensitivity as a function of characteristic structural length scale is evaluated. For both nanocrystalline and nanotwinned materials, the approach presented in this paper provides a unified model from envisioning partial dislocation emission for evaluating the three size-dependent parameters characterizing plastic deformation mechanism: flow stress, activation volume and strain-rate-sensitivity. This model also incorporates the possible effects of dislocation loop interactions, stress concentration and stacking faults. Predictions of the analysis are found to be generally consistent with experimental data. For the nanotwinned structures, where plastic deformation involves a competition between grain size and twin thickness effects, we generalize the non-uniform partial dislocation model [5] to express the flow stress explicitly in terms of grain size and twin thickness.
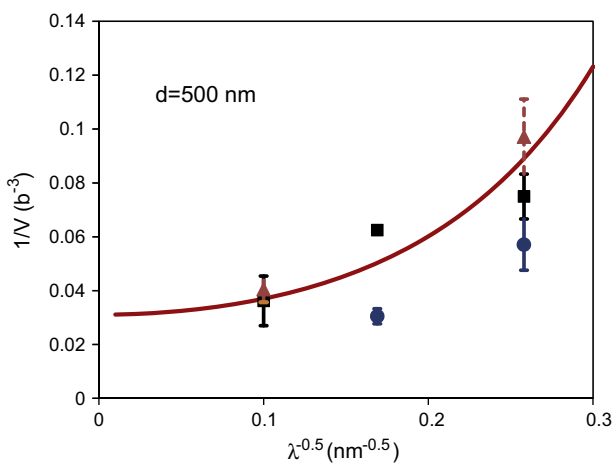
Fig. 7. Predicted and measured activation volume vs. twin thickness for nanotwinned Cu. The data are from Table 2 of Ref. [11]. The square symbols are from the nanoindentation test; the triangular symbols are from the jump test; the circle symbols are from the relaxation test.

By employing a methodology similar to that discussed in Ref. [28], where the side segments of partial dislocation loops are envisioned as contributing to rate sensitivity, the flow stress from the non-uniform partial dislocation model can be employed to develop a viscoplastic, rate-dependent constitutive relationship. The strain rate tensor resulting from the slip on the matrix slip plane is given as

$$\dot{\boldsymbol{\varepsilon}} = \sum \dot{\gamma} \mathbf{sm}, \tag{13}$$

where $\mathbf{s}$ is the unit vector along the Burgers vector and $\mathbf{m}$ is the unit normal of the matrix slip plane. The summation is over active slip systems. The shear strain rate on the matrix slip plane is

$$\dot{\gamma} = \begin{cases} \dot{\gamma}_0 \left(\dfrac{\tau - \tau_s}{g} \right)^{1/m} & \text{for } \tau - \tau_s > 0; \\ 0 & \text{for } \tau - \tau_s < 0. \end{cases} \tag{14}$$

Here $\dot{\gamma}_0$ is a reference strain rate and

$$g = \frac{G}{6} \left(\frac{b}{\lambda} + \frac{b}{d} \right); \tau_s = \frac{\Gamma}{b} - \frac{G}{24\pi\beta} \left(\frac{b}{\lambda} + \frac{b}{d} \right). \tag{15}$$

For slip on the twin plane, the shear strain rate $\dot{\gamma}$ is that obtained from Eq. (7). Such a rate-dependent and size-dependent three-dimensional constitutive relationship can be used to investigate the influence of grain size and twin thickness distributions to the deformation mechanism of nanoenhanced polycrystalline aggregates.

The present development does not address the potentially vital issue of the stability of either nanocrystalline or nanotwinned fcc structures. For instance, as shown by Zhang et al. [29] for nanocrystalline Cu (*via* microindentation) and by Liao et al. [30] for nanocrystalline Ni (*via* high-pressure torsion), nanoscale grains undergo severe coarsening when subjected to deformation under intense states of stress. Nanotwinned structures offer the prospect of far greater stability, due, in part, to the inherent low energy of coherent twin boundaries [31]. The optimality of nanotwinned structures vs. nanocrystalline structures has been explored *via* MD simulation by Kulkarni et al. [32], who later showed that not only were nanotwinned structures optimal, but that there was a ranking among fcc nanotwinned structures with respect to strength, ductility and stability. Recently, however, Fang et al. [33] have shown that gradient structures involving nanocrystalline and microcrystalline Cu can display attractive combinations of strength and ductility. The stability of such gradient structures was not explored, which still leaves open the question of optimality. Thus it would be useful to address in further work a "unified" methodology for comparing the expected behavior with respect to stability of nanocrystalline vs. nanotwinned fcc structures.

References

[1] Suresh S, Li J. Nature 2008;456:716–7.
[2] Asaro RJ, Krysl P, Kad B. Philos Mag Lett 2003;83:733–43.
[3] Asaro RJ, Suresh S. Acta Mater 2005;53:3369–82.
[4] Dao M, Lu L, Asaro RJ, De Hosson JTM, Ma E. Acta Mater 2007;55:4041–65.
[5] Gu P, Kad B, Dao M. Scripta Mater 2010;62:361–4.
[6] Lu L, Schwaiger R, Shan ZW, Dao M, Lu K, Suresh S. Acta Mater 2005;53:2169–79.
[7] Zhu T, Li J, Samanta A, Kim HG, Suresh S. PNAS 2007;104:3031–6.
[8] Asaro RJ, Kulkarni Y. Scripta Mater 2008;58:389–92.
[9] Lu L, Chen X, Huang X, Lu K. Science 2009;323:607–10.
[10] Lu L, Dao M, Zhu T, Li J. Scripta Mater 2009;60:1062–6.
[11] Lu L, Zhu T, Shen YF, Dao M, Lu K, Suresh S. Acta Mater 2009;57:5165–73.
[12] Lu K, Lu L, Suresh S. Science 2009;324:349–52.
[13] Van Swygenhoven H, Spaczer M, Caro A. Acta Mater 1999;47:3117–26.
[14] Conrad H. Metall Mater Trans A 2004;35:2681–95.
[15] Armstrong RW, Rodriguez P. Philos Mag 2006;86:5787–96.
[16] Conrad H. Nanotechnology 2007;18:325701.
[17] Hall EO. Proc Phys Soc London, Sect B 1951;64:747–53.
[18] Petch NJ. J Iron Steel Inst 1953;174:25–8.
[19] Dao M, Lu L, Shen YF, Suresh S. Acta Mater 2006;54:5421–32.
[20] Li X, Wei Y, Lu L, Lu K, Gao H. Nature 2010;464:877–80.
[21] Kulkarni Y, Asaro RJ. Acta Mater 2009;57:4835–44.
[22] Jin ZH, Gumbsch P, Ma E, Albe K, Lu K, Hahn H, et al. Scripta Mater 2006;54:1163–8.
[23] Jin ZH, Gumbsch P, Albe K, Ma E, Lu K, Gleiter H, et al. Acta Mater 2008;56:1126–35.
[24] Dewald MP, Curtin WA. Philos Mag 2007;87:4615–41.
[25] Schuh CA, Nieh TG, Iwasaki H. Acta Mater 2003;51:431–43.
[26] Van Vliet KJ, Tsikata S, Suresh S. Appl Phys Lett 2003;83:1441–3.
[27] Asaro RJ, Rice JR. J Mech Phys Solids 1977;25:309–38.
[28] Zhu B, Asaro RJ, Krysl P, Bailey R. Acta Mater 2005;53:4825–38.
[29] Zhang K, Weertman JR, Eastman JA. Appl Phys Lett 2006;87:061921.
[30] Liao XZ, Kilmametov AR, Valiev RZ, Gao H, Li X, Mukherjee AK, et al. Appl Phys Lett 2006;88:021909.
[31] Sutton AP, Ballufi RW. Interfaces in crystalline materials. Oxford: Oxford University Press; 1995.
[32] Kulkarni Y, Asaro RJ, Farkas D. Scripta Mater 2009;60:532–5.
[33] Fang TH, Li WL, Tao NR, Lu K. Science 2011;331:1587–90.